*remote sensing*

MDPI

*Article*

# High-Resolution Mapping of Shallow Water Bathymetry Based on the Scale-Invariant Effect Using Sentinel-2 and GF-1 Satellite Remote Sensing Data

**Jiada Guan [1,2], Huaguo Zhang [1,2,*], Tong Han [1,2], Wenting Cao [2], Juan Wang [2] and Dongling Li [2]**

[1] Ocean College, Zhejiang University, Zhoushan 316021, China; guanjd@zju.edu.cn (J.G.); hant@zju.edu.cn (T.H.)
[2] State Key Laboratory of Satellite Ocean Environment Dynamics, Second Institute of Oceanography, Ministry of Natural Resources, Hangzhou 310012, China; caowt@sio.org.cn (W.C.); wangjuan@sio.org.cn (J.W.); ldl@sio.org.cn (D.L.)
* Correspondence: zhanghg@sio.org.cn

**Abstract:** High-resolution water depth data are of great significance in island research and coastal ecosystem monitoring. However, the acquisition of high-resolution imagery has been a challenge due to the difficulties and high costs associated with obtaining such data. To address this issue, this study proposes a water depth inversion method based on Gaofen-1 (GF-1) satellite data, which integrates multi-source satellite data to obtain high-resolution bathymetric data. Specifically, the research utilizes bathymetric data derived from Sentinel-2 and Ice, Cloud, and Land Elevation Satellite-2 (ICESat-2) as prior information, combined with high-resolution imagery obtained from the GF-1 satellite constellation (GF-1B/C/D). Then, it employs a scale-invariant effect to map bathymetry with a spatial resolution of 2 m, applied to four study areas in the Pacific Islands. The results are further evaluated using ICESat-2 data, which demonstrate that the water depth inversion results from this study possess high accuracy, with $R^2$ values exceeding 0.85, root mean square error (RMSE) ranging from 0.56 to 0.90 m, with an average of 0.7125 m, and mean absolute error (MAE) ranging from 0.43 to 0.76 m, with an average of 0.55 m. Additionally, this paper discusses the applicability of the scale-invariant assumption in this research and the improvements of the quadratic polynomial ratio model (QPRM) method compared to the classical linear ratio model (CLRM) method. The findings indicate that the integration of multi-source satellite remote sensing data based on the scale-invariant effect can effectively obtain high-precision, high-resolution bathymetric data, providing significant reference value for the application of GF-1 satellites in high-resolution bathymetry mapping.

**Keywords:** bathymetry; GF-1; Sentinel-2; shallow water; scale-invariant effect

check for updates

Received: 2 January 2025
Revised: 8 February 2025
Accepted: 12 February 2025
Published: 13 February 2025

**Citation:** Guan, J.; Zhang, H.; Han, T.; Cao, W.; Wang, J.; Li, D. High-Resolution Mapping of Shallow Water Bathymetry Based on the Scale-Invariant Effect Using Sentinel-2 and GF-1 Satellite Remote Sensing Data. *Remote Sens.* **2025**, *17*, 640. https://doi.org/10.3390/rs17040640

**Copyright:** © 2025 by the authors. Licensee MDPI, Basel, Switzerland. This article is an open access article distributed under the terms and conditions of the Creative Commons Attribution (CC BY) license (https://creativecommons.org/licenses/by/4.0/).

## 1. Introduction

Bathymetric mapping is an important research direction in island research, involving various aspects such as navigation safety, fisheries, military applications, and nearshore engineering. Traditionally, light detection and ranging (LiDAR) systems were always used to map bathymetry in coastal areas [1,2]. However, in recent years, the rapid development of satellite-based optical remote sensing technology has provided some new solutions for bathymetric mapping in optical shallow water areas. This approach not only overcomes certain limitations of traditional depth measurement techniques that require ground-borne platforms but also offers advantages such as wide-area coverage and convenient data acquisition [3–9].

Considering the spatial heterogeneity of bathymetry, high-resolution bathymetric mapping images have always been of high research value in the field of bathymetric mapping [10]. Currently, available mainstream optical remote sensing data typically come from the Landsat series and the Sentinel-2 series, with spatial resolutions reaching 30 m and 10 m, respectively. Although the quality of these data is already quite high, the pursuit of higher resolution is still the goal of researchers. In order to obtain ultra-high-resolution images at the meter or even sub-meter level, it is usually necessary to rely on commercial satellite data such as Gaofen-2, GeoEye-1, Worldview-2/3, etc., but the high cost of these data limits their widespread application on a large scale.

The research of Collin [11] shows that although the value of each band in the fused red–green–blue (RGB) image no longer represents the true radiance or reflectance, reliable bathymetric information can still be extracted from the RGB image derived from Google Earth Pro through the statistical-based classical log-ratio model (CLRM). Based on this, this study proposes a scheme for obtaining high-resolution images through the fusion of Gaofen-1 satellite data, aiming to replace commercial satellite data for the inversion of high-resolution bathymetric images, with the goal of obtaining high-quality bathymetric data while controlling costs. This method provides an economical and efficient solution for high-resolution underwater topographic mapping.

The GF-1B/C/D satellite constellation (hereinafter referred to as GF-1 satellites) was launched by China on 31 March 2018, and contains three high-resolution optical satellites (GF-1B, GF-1C, and GF-1D) with the same performance and status, aiming at real-time monitoring of natural resources with full elements, full coverage, and all-weather conditions. The GF-1 satellites can provide panchromatic images with a spatial resolution of 2 m and multispectral images with a spatial resolution better than 8 m. Currently, optical satellite bathymetric methods are usually applied to water depths ranging from 0 to 20 m [12] and can be divided into two main categories: traditional multispectral empirical models and semi-analytical models. Traditional empirical models such as the basic linear models and the CLRM are relatively mature, but these methods heavily rely on in situ measurement data [7,13–15]. In contrast, semi-analytical models are based on radiative transfer theory and do not require in situ data; many researchers have developed various methods based on physical algorithms [16–19], though these methods have high requirements for imaging conditions and imaging quality.

While GF-1 satellite data have the advantage of high spatial resolution, the water depth inversion from single-scene images is limited by factors such as cloud cover and a lack of in situ water depth data, making it challenging to obtain high-quality water depth inversion results. When using Ice, Cloud, and Land Elevation Satellite-2 (ICESat-2) satellite bathymetric data as control points for water depth inversion, the low temporal resolution of GF-1 satellites and the fixed orbit of ICESat-2 result in an uncontrollable number of matching control points between different islands. In some island regions, there may not be enough control point data between the two ICESat-2 tracks for inversion. Therefore, this study considers combining other satellite data for multi-source data fusion to improve the quality of water depth inversion results. Liu et al. proposed a downscaling bathymetric mapping approach (DBMA) based on multi-temporal Landsat-8 images to obtain high-resolution water depth images in the absence of in situ water depth data [20]. Building on Collin's research, this method was further expanded into DBMA-RGB, which achieved the fusion of Landsat-8 images and RGB images exported from Google Earth Pro to produce ultra-high-resolution water depth images [10]. However, it was also noted that the significant resolution difference between Landsat-8 and RGB images could introduce errors. Therefore, this study considers combining the 2-m high spatial resolution images from GF-1 satellites with the 10-m images from Sentinel-2, which are closer in resolution, for water depth inversion, aiming to achieve more precise high-resolution water depth results.

This study is aimed at the issue of high costs associated with high-resolution satellite remote sensing imagery data, which makes it difficult to obtain high-resolution bathymetric data on a large scale. We propose a method based on scale-invariant effects to achieve high-resolution water depth inversion through multi-source data fusion. This method leverages the advantages of high-resolution images from GF-1 satellites and the abundant data from Sentinel-2 satellites, aiming to enhance the spatial resolution of bathymetric mapping. Specifically, we first fuse the remote sensing data from ICESat-2 and Sentinel-2 to invert and obtain lower-resolution bathymetric data. Then, based on scale-invariant effects, we apply downscaling techniques to ultimately achieve high-resolution bathymetric data at a spatial resolution of 2 m. We apply this method to four islands in the Pacific Island region and validate its effectiveness through ICESat-2 data. This study aims to demonstrate the feasibility and effectiveness of using GF-1B/C/D series satellite data for high-resolution bathymetric mapping through multi-source remote sensing data fusion, providing a reference for future related research. Additionally, we hope to further expand the application potential of GF-1 satellites in the field of bathymetric mapping.

## 2. Study Areas and Data

### *2.1. Study Areas*

The study area of this research is primarily concentrated in the Pacific Island region, which is characterized by rich ecosystems and a strong correlation between economic development and the ecological environment. There are a large number of islands and atolls in this region, but there is a lack of stable and reliable remote sensing data in this region due to the scattered distribution of islands and the vulnerability to cloudy and rainy weather conditions [21–23]. In this study, four islands or atolls within the region were selected as research objects, as shown in Figure 1.

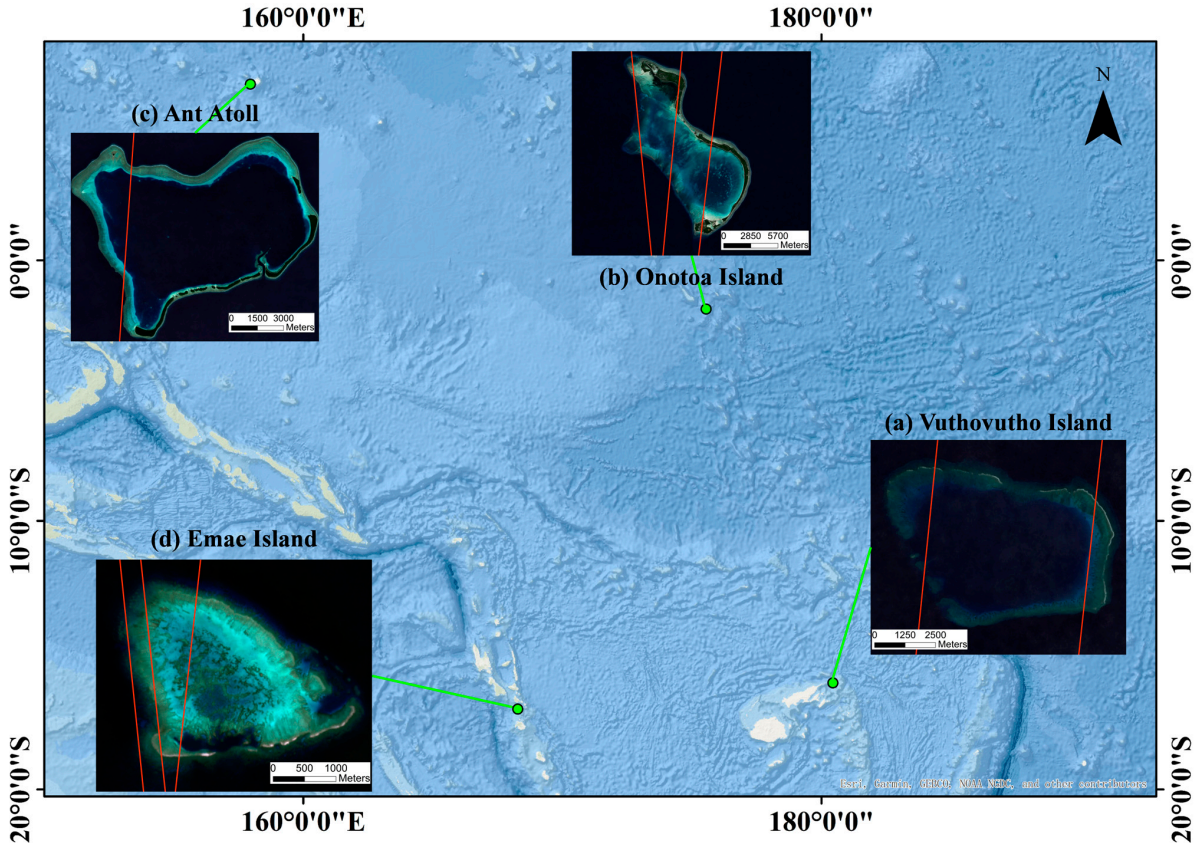



**Figure 1.** Distribution map of the four study areas, where the red solid line indicates the orbit of the ICESat-2 satellite.

### 2.2. Data

Three kinds of satellite data, GF-1, Sentinel-2, and ICESat-2, were used in this study, among which the GF-1 remote sensing images were obtained from the China Center for Resources Satellite Data and Application (CRESDA). The GF-1 images acquired in this study are all Level-1A raw data, which need to be pre-processed to derive surface reflectance data. The satellite IDs and image information of the GF-1 data used in this study are shown in Table 1.

**Table 1.** GF-1 data information and geographic location (latitude and longitude) of the four study areas.

| Study Area | Lat Lon | Satellite ID | Image ID | Imaging Time |
|---|---|---|---|---|
| Vuthovutho Island | 16.09°S 179.56°W | GF-1B | 1228298519 | 20 May 2023 |
| Onotoa Island | 1.88°S 175.55°E | GF-1D | 1257241855 | 22 June 2023 |
| Ant Atoll | 6.78°N 157.96°E | GF-1C | 1022061238 | 10 May 2023 |
| Emae Island | 17.06°S 168.28°E | GF-1D | 1257142905 | 9 November 2022 |

Sentinel-2 is a high-resolution multispectral imaging satellite launched by ESA, which carries a multispectral instrument that provides free multispectral image data with 10 m resolution. Due to the need for multi-year Sentinel-2 satellite imagery data in this study, the Google Earth Engine (GEE) platform was chosen as the basis for data access and processing, which is a large-scale cloud computing platform launched by Google Inc. to process satellite remote sensing image data and other Earth observation data. It provides a number of publicly available satellite image datasets, including Sentinel-2, and can quickly and efficiently obtain a large number of Sentinel-2 image data and process them quickly.

The ICESat-2 L2A data ATL03 dataset, which has been widely demonstrated to be applicable in shallow water bathymetry inversion [24–29], is also used in this study. However, due to the raw photons being very noisy, not all photons carry the correct height information, and even though ATL03 encodes the confidence level of all photons, it has been shown that there will still be some obvious underwater topographic signals that will be labeled as noise photons. Therefore, the improved density-based spatial clustering of applications with noise (DBSCAN) method proposed by Ma et al. [30] needs to be used for denoising before using the ICESat-2 data. In addition, since water depth is influenced by tidal levels, tidal correction is required for integrating ICESat-2 data from multiple dates. For this purpose, the Oregon State University Tidal Prediction Software (OTPS) with model TPXO7.2 was used to correct the tidal levels of each dataset to the same mean sea level and then merge them. Therefore, the vertical reference for water depth is based on the mean sea level.

## 3. Model and Methods

### 3.1. Workflow

To achieve high-resolution bathymetric inversion imagery, the bathymetric mapping in this study is divided into two parts. First, we employed a method that combines active and passive remote sensing data to fuse ICESat-2 data and Sentinel-2 data, resulting in bathymetric inversion at a spatial resolution of 10 m, which serves as prior data. Subsequently, to obtain high-resolution bathymetric results, it is necessary to combine the data with high-resolution fusion data from GF-1. After preprocessing the raw GF-1 data, the Nearest-neighbor diffusion-based pan-sharpening (NNDiffuse) method was employed to achieve a high-resolution fusion image at a resolution of 2 m. This image was then resampled to a spatial resolution of 10 m. A quadratic polynomial ratio model (QPRM) was fitted to derive the transformation equation, which was applied to the fused image based on

the scale-invariant assumption, ultimately resulting in high-resolution bathymetric imagery at a spatial resolution of 2 m. The specific workflow diagram is shown in Figure 2:

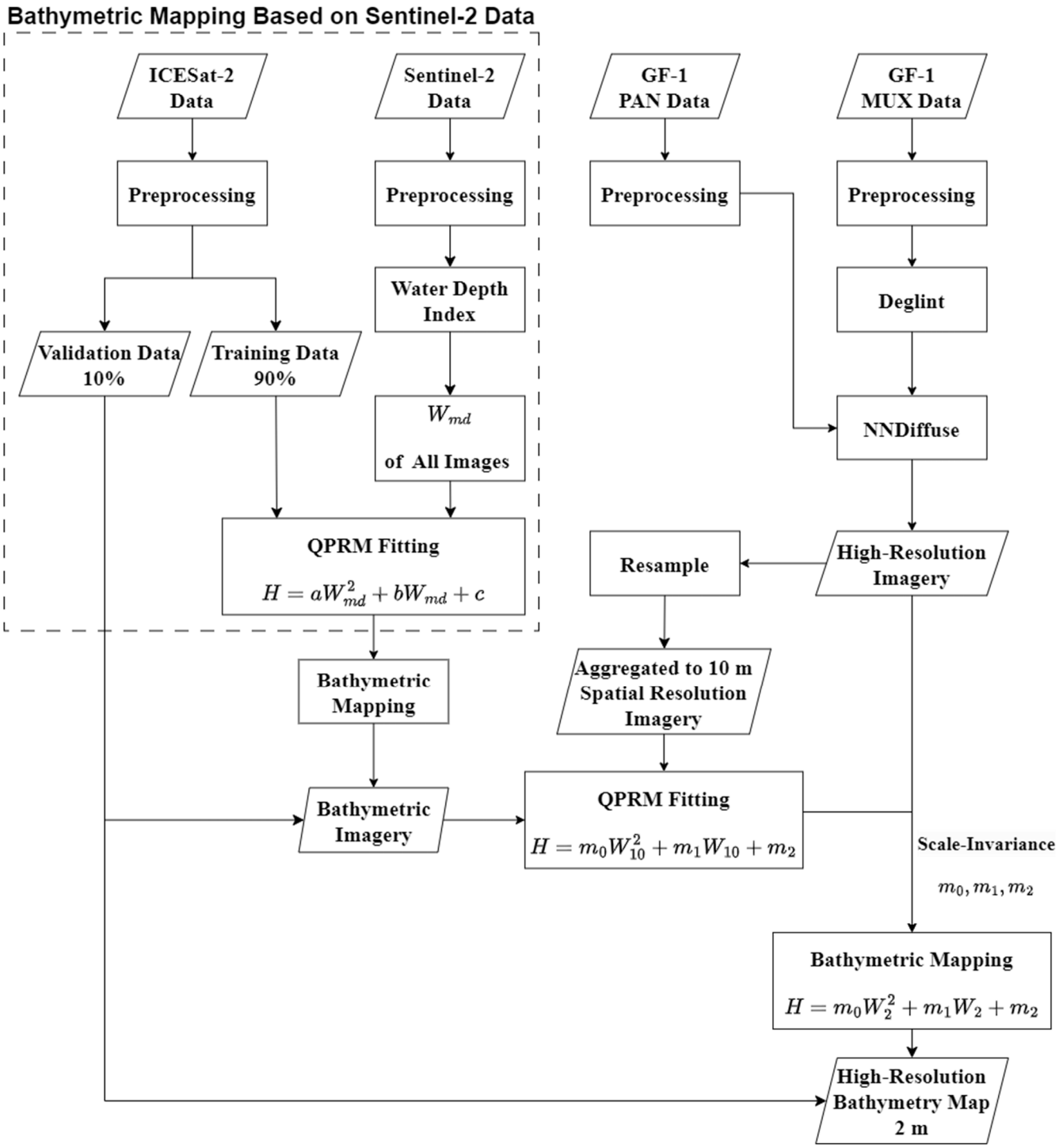



**Figure 2.** Workflow diagram of the bathymetric mapping.

### *3.2. Processing of Gaofen-1 Data*

For the GF-1 imagery data, the obtained data are initial digital number (DN) values, which require registration and radiometric calibration for the panchromatic data. The multispectral data also need to undergo preprocessing operations, including registration, radiometric calibration, and atmospheric correction, to derive surface reflectance data. Since there is currently a lack of targeted atmospheric correction methods for GF-1 satellites,

this study employs the 6S atmospheric correction method proposed by Vermote et al. [31], which has good general applicability. The image-related parameters required for this method can be obtained from the accompanying XML attribute table, while aerosol optical thickness data AOT550 can be computed using Aerosol Robotic Network (AERONET) (https://aeronet.gsfc.nasa.gov (accessed on 29 July 2024)) data.

In ocean remote sensing, the mirror reflection of sunlight on the rough sea surface (sun glint) is a strong interference signal, and the presence of sun glint also introduces errors when carrying out bathymetric mapping inversion, so it must be suppressed. In this study, we employed the remote sensing correction method proposed by Hedley et al. [32] in 2005 to perform deglint on the multispectral data. The specific mathematical relationship is as follows:

$$\rho_{SR}^{deg}(\lambda) = \rho_{SR}(\lambda) - b_\lambda(\rho_{NIR} - MIN\rho_{NIR}) \quad (1)$$

where $\lambda$ represents the central wavelength of each band, $\rho_{SR}^{deg}$ is the surface reflectance after deglint, $\rho_{SR}$ is the initial surface reflectance data corresponding to the central band, $\rho_{NIR}$ is the surface reflectance in the near-infrared band, $MIN\rho_{NIR}$ is the minimum value of near-infrared band reflectance within a given area, and $b_\lambda$ is the undetermined linear coefficient between the visible band corresponding to the central band and the near-infrared band.

Finally, the processed panchromatic and multispectral images were fused using the NNDiffuse algorithm proposed by Sun et al. This method treats the spectrum as the minimum element, allowing for better preservation of spatial and spectral characteristics, which facilitates the detailed feature extraction of satellite images [33].

### *3.3. Bathymetric Mapping Based on Active-Passive Remote Sensing Data*

Han et al. [25] proposed a bathymetric mapping method based on a large amount of active and passive remote sensing data to remove the effects of complex underwater optical paths and sea surface instabilities on satellite images. This method integrates several years of ICESat-2 data with Sentinel-2 data, enabling large-scale and efficient bathymetric mapping in the absence of in situ data. Specifically, in this study, available Sentinel-2 and ICESat-2 data from 2019 to 2022 were selected. The ICESat-2 data undergo a series of preprocessing steps, including DBSCAN denoising, tidal correction, and multi-orbit data fusion, to serve as prior data. The resulting available ICESat-2 data were then partitioned into training and validation datasets. Subsequently, L2A data from Sentinel-2 are directly accessed online via the GEE platform. Clouds and cloud shadows are removed based on the Cloud Score+ QA band [34], and glint correction is applied. For the extensive Sentinel-2 dataset, the median value $W_{md}$ of the Water Depth Index (WDI) for each pixel is calculated, and the coefficients of the QPRM are fitted through combination with the ICESat-2 training datasets, resulting in bathymetric inversion imagery with a spatial resolution of 10 m.

### *3.4. Statistical-Based Bathymetric Method*

Initially, Stumpf et al. [7] proposed the CLRM, and then Collin [11] showed that reliable bathymetric information can still be extracted from fused RGB images based on the CLRM; the DBMA-RGB method proposed by Liu et al. [10] also demonstrated the feasibility of applying the model on RGB images. The mathematical formula of the model is expressed as follows.

$$H = m_0 W + m_1 \quad (2)$$

$$W = \frac{ln(qR_{rs}(Band_1))}{ln(qR_{rs}(Band_2))} \quad (3)$$

where $H$ represents water depth, while $m_0$ and $m_1$ are two unknown constants, $W$ denotes the water depth index, and $q$ is a constant that ensures the logarithmic expression is mean-

ingful, typically set to 10,000. $R_{rs}(Band_1)$ and $R_{rs}(Band_2)$ refer to the surface reflectance data of two bands in the imagery. By selecting appropriate spectral combinations, water depth can be effectively modeled. Currently, a commonly used combination in the field of bathymetry involves using the blue band for $Band_1$ and the green band for $Band_2$.

This linear model is the most widely used statistical model in bathymetric inversion, but Han et al. suggested that the results of this linear model are unsatisfactory in the actual bathymetric inversion process, especially in the inversion of shallow water areas, and thus proposed the QPRM instead of the traditional linear model for bathymetric inversion [25]. Its mathematical formula is expressed as follows:

$$H = m_0 W^2 + m_1 W + m_2 \tag{4}$$

where $m_0$, $m_1$, and $m_2$ are all constants to be determined by fitting. Specifically, in this research, water depth imagery at a spatial resolution of 10 m was first obtained based on the water depth mapping method introduced in Section 3.3, using this water depth data as control data. Next, the water depth index in 10 m $W_{10}$ was calculated through Formula (3) for the 10-m spatial resolution imagery obtained from the resampled GF-1 fused data. The two datasets were then paired to construct a training dataset. To improve the quality of the dataset, anomalous data pairs in the GF-1 data that may be affected by clouds or cloud shadows were manually removed through visual interpretation. After that, a set of coefficients, $m_0$, $m_1$, and $m_2$, at the 10-m spatial resolution can be fitted by QPRM. Finally, the water depth index in 2 m $W_2$ was calculated for the 2-m GF fused data, and based on the scale-invariant effect, the fitted coefficients obtained earlier were directly applied in the QPRM, achieving high-resolution water depth mapping at a spatial resolution of 2 m.

### *3.5. Validation*

In this study, separate model training and depth mapping were conducted for each research area. Due to the lack of in situ depth data that could serve as ground truth for validation, we evaluated the accuracy of the inversion results from our method by isolating a portion of the available ICESat-2 data for accuracy verification. The assessment was carried out using scatter plots, linear regression lines, correlation coefficients ($R^2$), root mean square error (RMSE), and mean absolute error (MAE) between the ICESat-2 data and the depth results based on GF-1. The RMSE and MAE were calculated using the following formulas:

$$RMSE = \sqrt{\sum_{i=1}^{m} \frac{(H_G - H_I)^2}{m}} \tag{5}$$

$$MAE = \frac{1}{m} \sum_{i=1}^{m} |H_G - H_I| \tag{6}$$

where $H_G$ represents the water depth data obtained through the proposed method based on GF-1 fusion data, while $H_I$ denotes the ICESat-2 depth measurement results used for validation. The variable $m$ indicates the number of ICESat-2 data points available for validation in each study area.

## 4. Results

### *4.1. Complete Islands Mapping Results*

As shown in Figure 3, the water depth inversion results for the four study areas within the 0–20 m depth range are presented. The figure displays both the overall water depth inversion results for each island and the detailed characteristics of local areas, comparing them with the water depth inversion results based on Sentinel-2 data proposed by Han et al. It can be observed from the figure that the water depth results obtained from the

two methods are generally similar. However, in some edge areas of the islands, the results from this study appear to be slightly lower, which may be related to the presence of cloud cover and wave effects at the edges of the islands. Nevertheless, upon examining the local details of the islands, it becomes evident that this study's method, due to its higher spatial resolution, is able to depict underwater topographic features more clearly and coherently, showcasing richer terrain information.

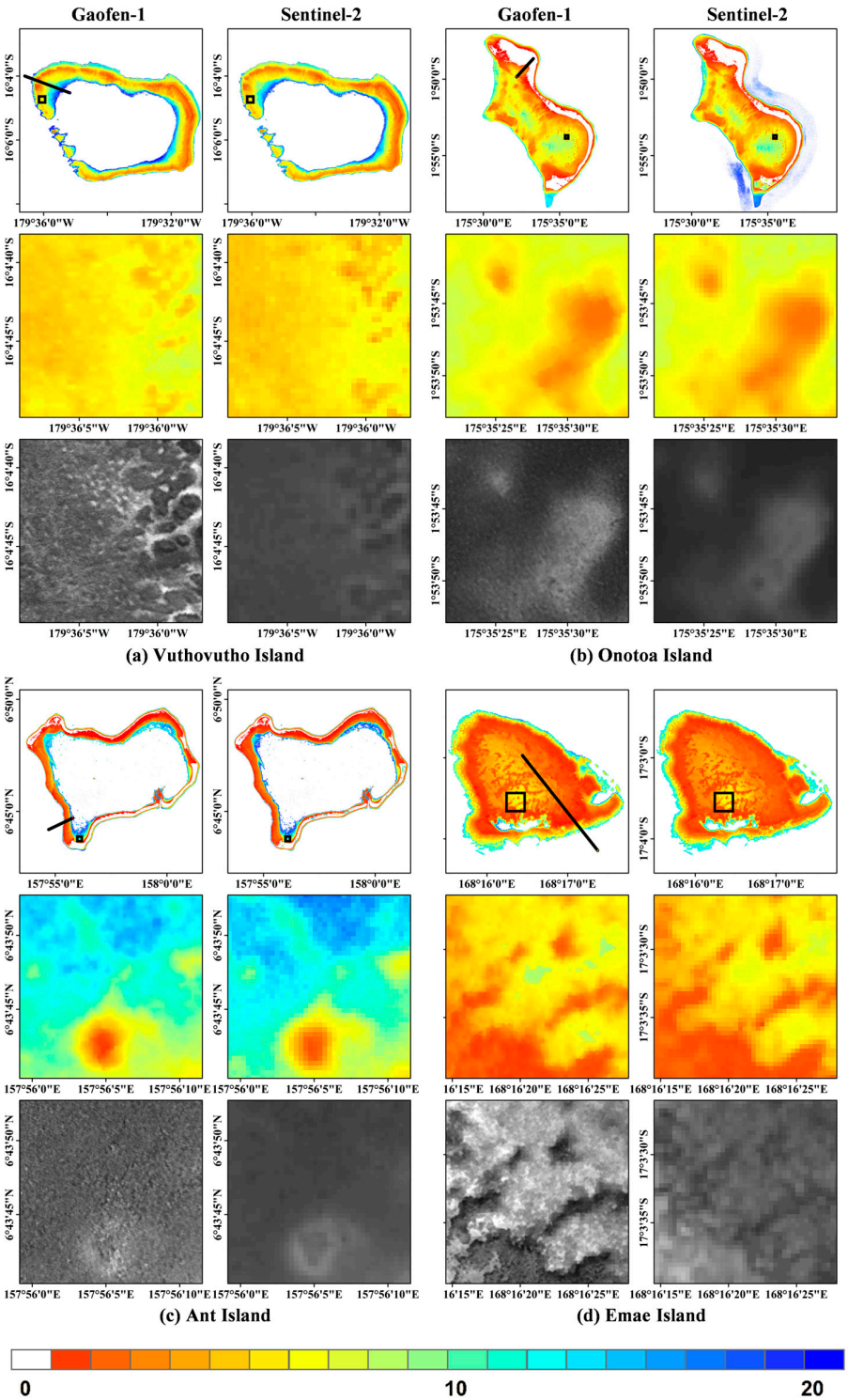



**Figure 3.** Complete bathymetric mapping results based on Sentinel-2 and GF-1 inversions for the four study areas (**top**), detailed bathymetric results for localized areas (**middle**), and original imagery (**bottom**); the black boxes indicate the specific location of the localized results on the complete island and the solid black lines indicate the location of the profiles used for analysis in Figure 4.

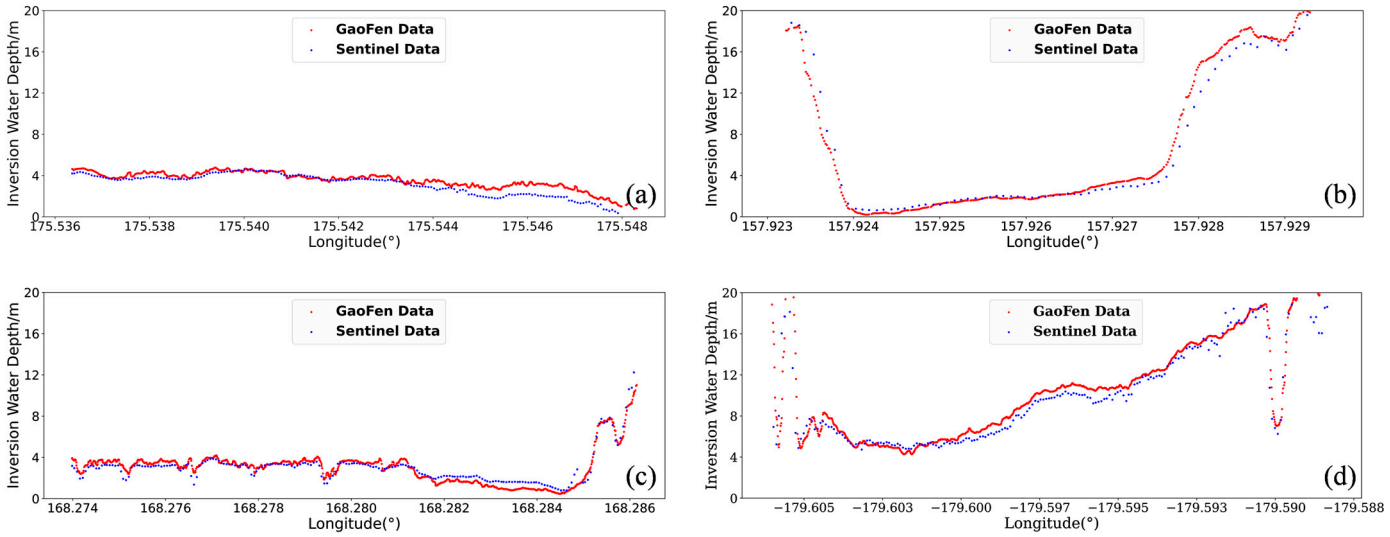



**Figure 4.** Scatterplot comparison of profiles in the four study areas: (**a**) Onotoa Island; (**b**) Ant Atoll; (**c**) Emae Island; (**d**) Vuthovutho Island.

To demonstrate more intuitively the effect of the improved resolution, a profile was selected from each island in each study area to compare the differences in the bathymetric results obtained by inversion using Sentinel-2 data and GF-1 data. As shown in Figure 4, it can be seen from the profiles that although the overall trend of the bathymetry results obtained by the two methods is similar, the results obtained based on the GF-1 data in this study have a significantly higher density of points in the profile, which is able to depict the fluctuating characteristics of the local bathymetry changes in a more detailed way compared with the Sentinel-2 inversion results.

### *4.2. Accuracy Validation*

To comprehensively evaluate the accuracy of the water depth results obtained from GF-1, the retrieved water depth data were validated using ICESat-2 data, and a scatter plot was generated. The validation results are illustrated in Figure 5. From the figure, it can be observed that within the water depth range of 0–20 m across the four study areas, the average $R^2$ value is 0.9266, the average RMSE is 0.7125 m, and the average MAE is 0.55 m. Although a small number of outliers can still be observed on some islands in the figure, these errors are likely due to the inherent limitations of the DBSCAN method in denoising from ICESat-2 data, which are considered unavoidable systematic errors. Further processing of the bathymetric data may be required [30]. However, overall, the validation results indicate that the inversion results obtained from this study indicate a high level of correlation and low error levels, demonstrating the effectiveness and reliability of this method.

Among the four study areas, the bathymetric inversion results of Emae Island exhibit the best performance, with an RMSE of 0.56 m and an MAE of 0.43 m, significantly outperforming the other regions. This indicates that the method employed in this study is capable of effectively capturing the actual variations in water depth in this area, demonstrating high spatial accuracy. Furthermore, the fitted curves in the scatter plots for all study areas are generally close to the 1:1 line, with $R^2$ values exceeding 0.85. This suggests a high level of accuracy in the water depth inversion results, with minimal differences between the predicted values and the true values. Overall, through comparisons with ICESat-2 data, the water depth inversion method proposed in this study demonstrates strong adaptability and reliability, effectively retrieving water depth information and showing broad application prospects.

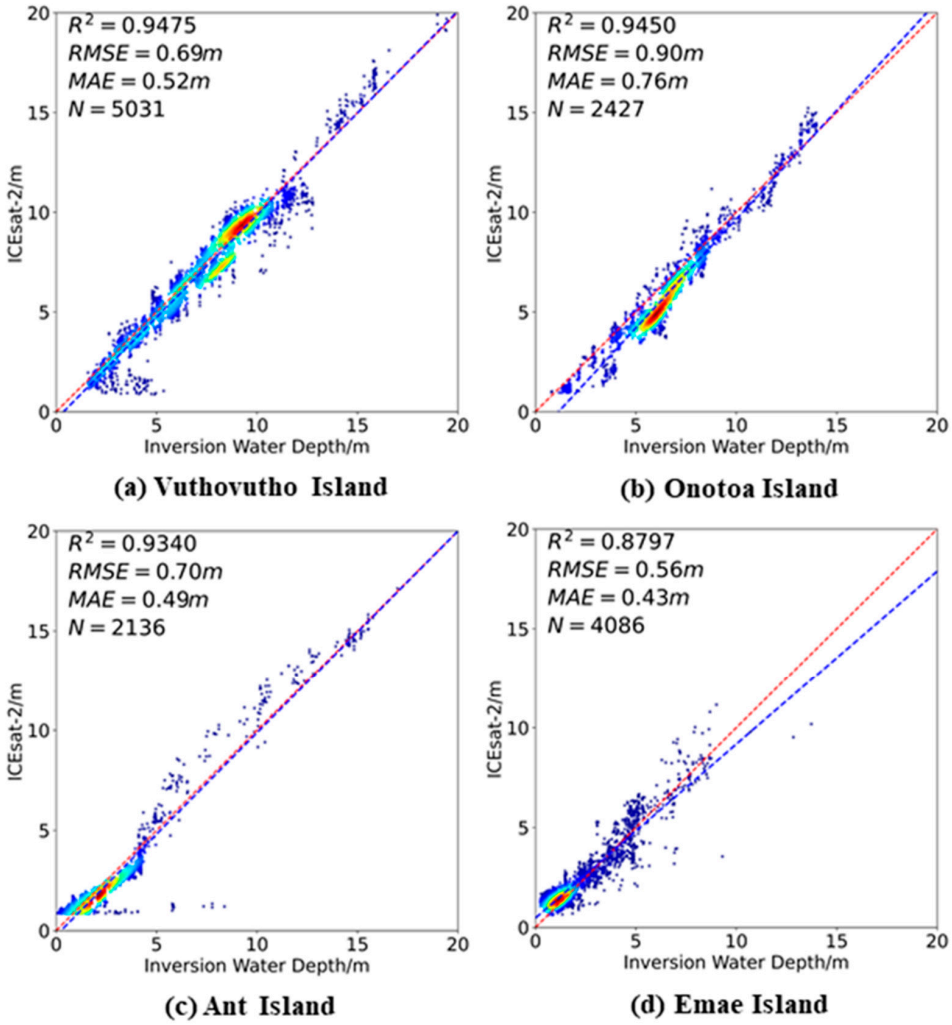



**Figure 5.** Comparison results of bathymetric data obtained from inversion with ICESat-2 data in the four islands, where the red dashed line is the 1:1 line, the blue dashed line is the fitted line, and N is the number of data points from ICESat-2 used for validation.

## 5. Discussion

### *5.1. Scale-Invariant Assumption*

The scale-invariance assumption is a core hypothesis in this study's methodology. Its fundamental concept is that statistical models established using low spatial resolution images or large-scale data can continue to be applicable to high spatial resolution or small-scale imagery. Scale issues have long been one of the most important research focuses in the field of remote sensing [35]. Building on previous studies, many scholars have widely applied the scale-invariance hypothesis to various research areas, such as land surface temperature retrieval, and have demonstrated the hypothesis's strong applicability [36,37]. In order to verify the applicability of this assumption in the methodology of this study, a set of parallel sections are uniformly plotted on each island in this study to compare the 2-m resolution bathymetry data obtained from the inversion based on the GF data with the 10-m-resolution bathymetry data obtained from the inversion based on the Sentinel-2 data. The specific sampling method is: from the westernmost to the easternmost side of the island, a set of north–south section straight lines are selected every 1000 m, and uniform sampling points are generated on each section with 10-m resolution (Figure A1). The final obtained bathymetry data were presented through a scatterplot, as shown in Figure 6. From the scatter plot, it can be observed that the water depth results retrieved using the proposed method

exhibit a high correlation with the water depth data obtained from Sentinel-2, with $R^2$ values exceeding 0.91. Additionally, the high-density data points across the four study areas are approximately aligned with the 1:1 line, and the slope of the fitted line approaches 1. This indicates that the statistical model established based on 10-m spatial resolution data remains effective in reflecting water depth information when applied to 2-m spatial resolution GF data, thereby validating the applicability of the scale-invariance hypothesis in this study.

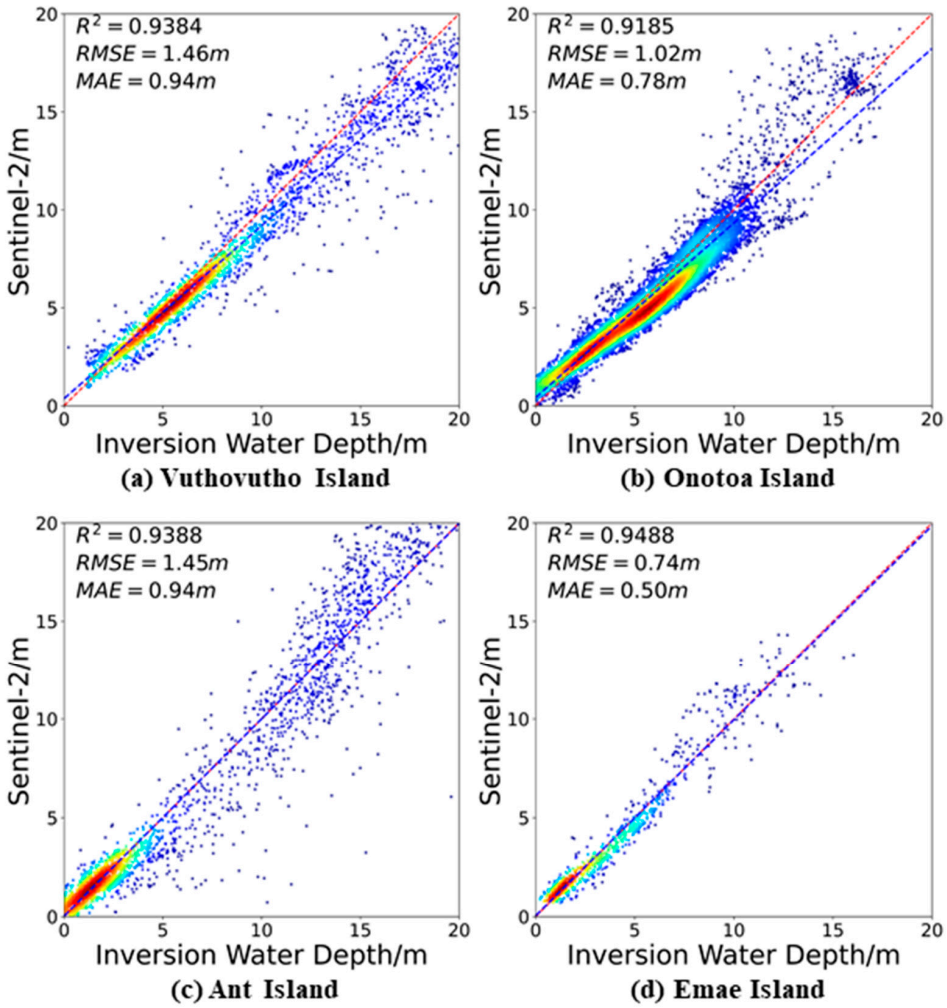



**Figure 6.** Comparison of the bathymetric data results obtained from GF-1 data and from Sentinel-2 data, where the red dashed line represents the 1:1 line and the blue dashed line indicates the fitted line.

However, the scatter also reveals some discrepancies between the two methods, suggesting that there is still room for improvement in the water depth results obtained in this study. This discrepancy may be attributed to the fact that the method proposed by Han et al. utilizes multi-year median composite images from Sentinel-2 for water depth retrieval, whereas the method in this study is based on single-scene GF-1 image data. The accuracy of the retrieval is thus dependent on the imaging quality of the single scene. Han et al. [20] also mentioned the effectiveness of increasing the number of images for improving accuracy, which represents one of the potential directions for enhancing the method proposed in this study.

### *5.2. Comparison of the QPRM and CLRM*

In this study, the QPRM was used to replace the most commonly used CLRM for water depth inversion of GF data. The comparison results in Table 2 indicate that the water depth results obtained using the CLRM, when compared to ICESat-2 data, yielded an average $R^2$ of 0.9199, an average RMSE of 0.825 m, and an average MAE of 0.65 m. Under the

same conditions, the inversion results of the QPRM demonstrated superior performance across all evaluation metrics, generally outperforming the CLRM. Notably, in the study areas of Onotoa Island and Ant Atoll, the QPRM showed particularly outstanding results, with RMSE improvements of 10.89% and 27.08%, respectively, and MAE improvements of 11.63% and 30.99%. These results indicate that the application of the QPRM in this study offers significant advantages, providing more accurate water depth inversion results.

**Table 2.** The table presents a comparison of the fitting results between the CLRM and the QPRM, where the subscript "Q" denotes the fitting results of the QPRM and the subscript "L" denotes the fitting results of the CLRM.

| Study Area | $R_Q^2/R_L^2$ | $RMSE_Q/RMSE_L$ | $MAE_Q/MAE_L$ |
|---|---|---|---|
| Vuthovutho Island | 0.9475/0.9429 | 0.69/0.72 | 0.52/0.55 |
| Onotoa Island | 0.9424/0.9288 | 0.90/1.01 | 0.76/0.86 |
| Ant Atoll | 0.9340/0.9313 | 0.70/0.96 | 0.49/0.71 |
| Emae Island | 0.8797/0.8765 | 0.56/0.61 | 0.43/0.48 |

### *5.3. Advantages of Using Gaofen-1 Fusion Data as a Substitute for Traditional RGB Imagery Acquisition Methods for High-Resolution Data*

The RGB imageries directly available in traditional application platforms (e.g., Google Earth Pro) usually contain only red, green, and blue bands, which cannot effectively eliminate the sun glint signals in the images, and the interference of sun glint on the bathymetric inversion results has been confirmed by several studies [32,38,39]. Therefore, in this study, we adopt the method of fusing GF-1 data by ourselves instead of the traditional direct download of RGB imageries to obtain high-resolution image data, and introduce a deglint step in the pre-processing of GF-1 multispectral images, and then fuse them to obtain high-resolution image data after removing the sun glint signals.

Furthermore, Liu et al. noted in their research [10,20] that commercially available RGB imagery data often come from various satellite sensors. This not only leads to inconsistencies in the resolution of the obtained bathymetric data but also introduces uncertainties due to spectral differences between different sensors, which may affect the accuracy of the inversions. In light of this, this study focuses on water depth inversion using data from the GF-1 satellite series exclusively. This strategy not only avoids the uncertainties introduced by multiple sensors but also ensures consistency in the resolution of the final inversion results. It can provide a reference for the future application and promotion of GF-1 satellite data in water depth mapping.

## 6. Conclusions

This study proposes a high-resolution water depth inversion method based on GF-1 satellite data, utilizing the scale-invariant effect to successfully achieve water depth inversion at a spatial resolution of 2 m. This method not only enhances the spatial resolution of bathymetry mapping but also provides an innovative solution for the economical and efficient mapping of underwater topography. The research results indicate that, compared to the water depth results derived from Sentinel-2 data, the water depth data inverted from GF-1 exhibit a similar overall trend. Although there are instances of underestimation at the edges of certain islands, the GF-1 data present a more detailed and richer depiction of local water depth features. Furthermore, the accuracy was evaluated by comparison with ICESat-2 data. The results showed that the $R^2$ values of the four study areas were all greater than 0.85, the RMSE ranged from 0.56 to 0.90 m, with an average of 0.7125 m, and the MAE ranged from 0.43 to 0.76 m, with an average of 0.55 m, which further verified the reliability of this research method in water depth inversion.

In addition, this study also explores the applicability of the scale-invariance assumption and compares the effect of using the QPRM to replace the traditional CLRM, and the

results show that QPRM demonstrates a significant improvement within the framework of this study, which further proves the effectiveness and innovation of the proposed method and demonstrates the promising prospect of the GF-1 satellite data in bathymetric mapping.

However, this study does have some limitations. Firstly, due to the temporal resolution of the GF-1 satellite and the climatic conditions characterized by frequent cloud cover and rain in the Pacific Island region, the number of effective images from the GF-1 satellite in the Pacific area is quite limited. This study exclusively employed single-scene GF-1 imagery for bathymetric inversion. It should be noted that the accuracy of such single-scene-derived results is inherently constrained by image quality factors, which may introduce certain uncertainties. Second, the current preprocessing methods for GF-1 satellite data are not well developed, lacking a systematic and dedicated approach for quality control specific to this satellite series. This may affect both the image quality and the final water depth inversion results. To address these issues, future research could focus on developing more comprehensive image quality control and preprocessing methods or exploring multi-temporal data fusion techniques to enhance the quality of remote sensing imageries and improve the accuracy of water depth inversions.

On the other hand, since the study area of this research is primarily focused on Pacific Island countries, and there is a lack of extensive and reliable in situ bathymetric data in this region, the research results presented in this paper could not be directly validated against in situ bathymetric data. Therefore, we could only refer to previous water depth inversion results and ICESat-2 data to assess the feasibility of the methods employed in this study. Nevertheless, the research indicates that this method has strong application potential, and future studies could be conducted in more regions, incorporating in situ data to validate and optimize the method, thereby enhancing its applicability and accuracy.

Overall, this study offers a new approach and methodology for high-resolution remote sensing water depth inversion in shallow water areas and demonstrates the potential application of GF-1 satellite data in high-resolution water depth inversion. Future efforts could focus on further optimizing the data processing workflow and expanding the study area to promote the application of this research method in water depth mapping.

**Author Contributions:** Conceptualization, H.Z.; methodology, J.G., T.H. and H.Z.; software, J.G.; validation, J.G.; formal analysis, J.G.; data curation, J.G. and T.H; writing—original draft preparation, J.G.; writing—review and editing, H.Z.; visualization, J.G.; supervision, H.Z.; project administration, J.W., W.C. and D.L.; funding acquisition, H.Z. All authors have read and agreed to the published version of the manuscript.

**Funding:** This research was funded in part by the National Key Research and Development Program of China, grant number 2021YFE0117600.

**Data Availability Statement:** The raw data supporting the conclusions of this article will be made available by the authors on request.

**Acknowledgments:** This research was partially supported by the National Key Research and Development Program (Grant No. 2021YFE0117600), for which we are grateful. We would also like to express our sincere appreciation to the CRESDA for their support in this study, particularly for providing a substantial amount of GF-1B/C/D imagery data and assistance with image preprocessing. Additionally, we extend our heartfelt thanks to Google for providing the GEE platform and to the European Space Agency for supplying Sentinel-2 satellite imagery data. Finally, we thank the AERONET jointly established by NASA and LOA-PHOTONS (CNRS) for providing the aerosol optical thickness data required for atmospheric correction in this study.

**Conflicts of Interest:** The authors declare no conflicts of interest.

## Abbreviations

The following abbreviations are used in this manuscript:

| | |
|---|---|
| AERONET | Aerosol Robotic Network |
| CLRM | Classical linear ratio model |
| CRESDA | China Center for Resources Satellite Data and Application |
| DBMA | Downscaling bathymetric mapping approach |
| DBSCAN | Density-based spatial clustering of applications with noise |
| DN | Digital number |
| GEE | Google Earth Engine |
| ICESat-2 | Ice, Cloud, and Land Elevation Satellite-2 |
| LiDAR | Light detection and ranging |
| NNDiffuse | Nearest-neighbor diffusion-based pan-sharpening |
| QPRM | Quadratic polynomial ratio model |
| RGB | Red–green–blue |
| WDI | Water depth index |

## Appendix A

Figure A1 presents the profiles for sampling Sentinel-2 and GF-1 data mentioned in Section 5.1. Specifically, the profiles extend from the westernmost to the easternmost point of the island, with profiles generated at 1 km intervals. Sampling points are evenly distributed along each profile at 10 m intervals.

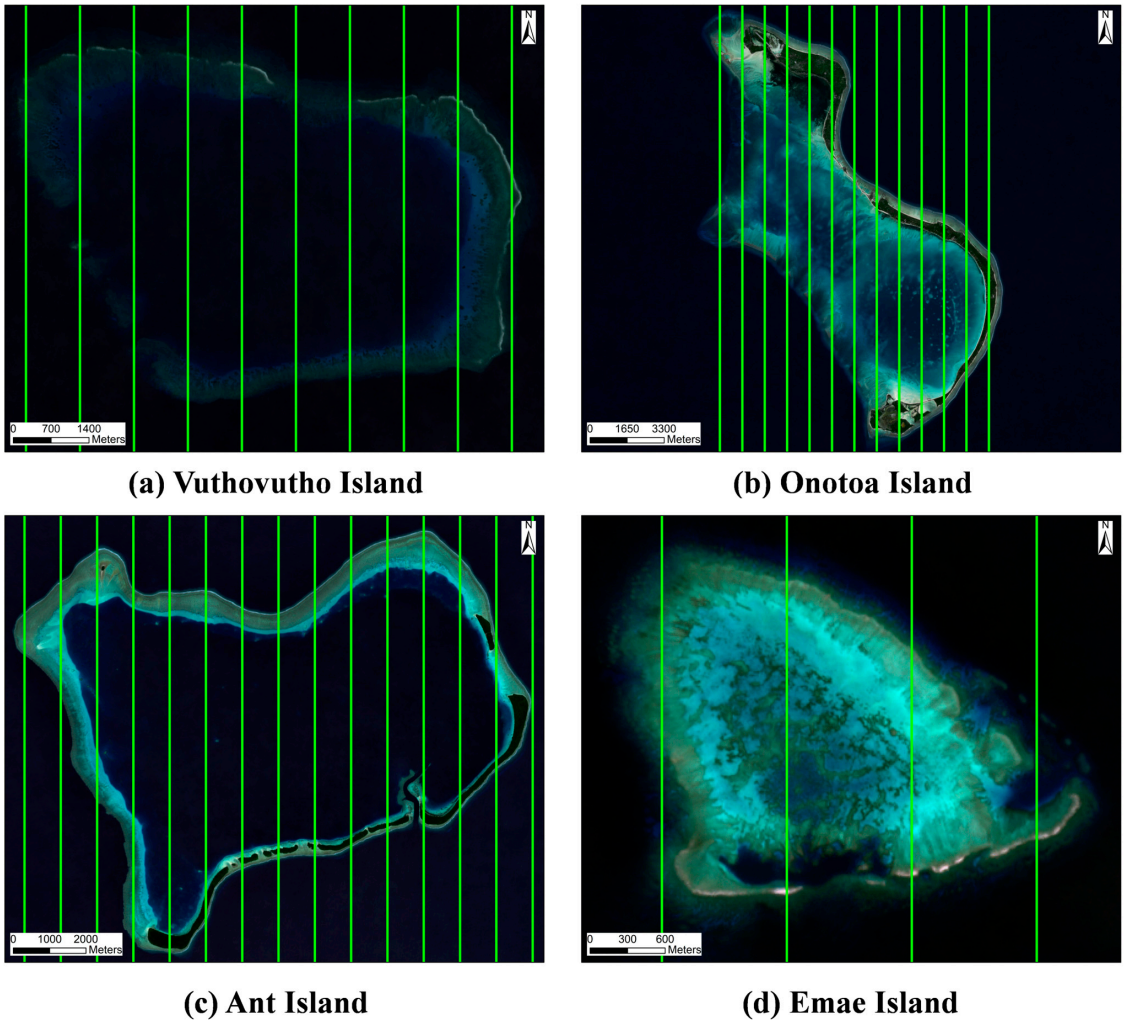



**Figure A1.** The location of profiles selected on each island used for discussing the scale-invariant assumption in Section 5.1, where the interval between each two profiles is 1 km.

## References


1. Yeu, Y.; Yee, J.-J.; Yun, H.S.; Kim, K.B. Evaluation of the Accuracy of Bathymetry on the Nearshore Coastlines of Western Korea from Satellite Altimetry, Multi-Beam, and Airborne Bathymetric LiDAR. *Sensors* **2018**, *18*, 2926. [CrossRef]
2. Takhtkeshha, N.; Mandlburger, G.; Remondino, F.; Hyyppä, J. Multispectral Light Detection and Ranging Technology and Applications: A Review. *Sensors* **2024**, *24*, 1669. [CrossRef] [PubMed]
3. Lai, W.; Lee, Z.; Wang, J.; Wang, Y.; Garcia, R.; Zhang, H. A Portable Algorithm to Retrieve Bottom Depth of Optically Shallow Waters from Top-Of-Atmosphere Measurements. *J. Remote Sens.* **2022**, *2022*, 9831947. [CrossRef]
4. Lee, Z.; Carder, K.L. Hyperspectral Remote Sensing of Shallow Water Environments: A Review. *Hyperspectral Remote Sens. Ocean.* **2001**, *4154*, 83–94.
5. Hedley, J.; Roelfsema, C.; Phinn, S.R. Efficient Radiative Transfer Model Inversion for Remote Sensing Applications. *Remote Sens. Environ.* **2009**, *113*, 2527–2532. [CrossRef]
6. Bergsma, E.W.J.; Almar, R.; Rolland, A.; Binet, R.; Brodie, K.L.; Bak, A.S. Coastal Morphology from Space: A Showcase of Monitoring the Topography-Bathymetry Continuum. *Remote Sens. Environ.* **2021**, *261*, 112469. [CrossRef]
7. Stumpf, R.P.; Holderied, K.; Sinclair, M. Determination of Water Depth with High-Resolution Satellite Imagery over Variable Bottom Types. *Limnol. Oceanogr.* **2003**, *48*, 547–556. [CrossRef]
8. Cao, B.; Deng, R.; Zhu, S. Universal Algorithm for Water Depth Refraction Correction in Through-Water Stereo Remote Sensing. *Int. J. Appl. Earth Obs. Geoinf.* **2020**, *91*, 102108. [CrossRef]
9. Goodman, J.A.; Purkis, S.J.; Phinn, S.R. Coral Reef Remote Sensing. In *A Guide for Mapping, Monitoring and Management*; Springer: Berlin/Heidelberg, Germany, 2013; 436p.
10. Liu, Y.; Tang, S.; Deng, R.; Huang, Y.; Ye, H.; Xu, Z.; Zeng, K. Mapping Ultrahigh-Spatial-Resolution Bathymetry for a Wide Range of Coastal Optically Shallow Waters Without In Situ Bathymetric Data. *IEEE Trans. Geosci. Remote Sens.* **2023**, *61*, 4207716. [CrossRef]
11. Collin, A.; Nadaoka, K.; Nakamura, T. Mapping VHR Water Depth, Seabed and Land Cover Using Google Earth Data. *ISPRS Int. J. Geo-Inf.* **2014**, *3*, 1157–1179. [CrossRef]
12. Chen, B.; Yang, Y.; Xu, D.; Huang, E. A Dual Band Algorithm for Shallow Water Depth Retrieval from High Spatial Resolution Imagery with No Ground Truth. *ISPRS J. Photogramm. Remote Sens.* **2019**, *151*, 1–13. [CrossRef]
13. Lyzenga, D.R. Passive Remote Sensing Techniques for Mapping Water Depth and Bottom Features. *Appl. Opt.* **1978**, *17*, 379. [CrossRef]
14. Lyzenga, D.R. Shallow-Water Bathymetry Using Combined Lidar and Passive Multispectral Scanner Data. *Int. J. Remote Sens.* **1985**, *6*, 115–125. [CrossRef]
15. Lyzenga, D.R.; Malinas, N.P.; Tanis, F.J. Multispectral Bathymetry Using a Simple Physically Based Algorithm. *IEEE Trans. Geosci. Remote Sens.* **2006**, *44*, 2251–2259. [CrossRef]
16. Lee, Z.; Carder, K.L.; Mobley, C.D.; Steward, R.G.; Patch, J.S. Hyperspectral Remote Sensing for Shallow Waters I A Semianalytical Model. *Appl. Opt.* **1998**, *37*, 6329. [CrossRef] [PubMed]
17. Lee, Z.; Carder, K.L.; Mobley, C.D.; Steward, R.G.; Patch, J.S. Hyperspectral Remote Sensing for Shallow Waters: 2 Deriving Bottom Depths and Water Properties by Optimization. *Appl. Opt.* **1999**, *38*, 3831. [CrossRef] [PubMed]
18. Lee, Z.; Carder, K.L. Effect of Spectral Band Numbers on the Retrieval of Water Column and Bottom Properties from Ocean Color Data. *Appl. Opt.* **2002**, *41*, 2191. [CrossRef] [PubMed]
19. Ma, Y.; Zhang, H.; Li, X.; Wang, J.; Cao, W.; Li, D.; Lou, X.; Fan, K. An Exponential Algorithm for Bottom Reflectance Retrieval in Clear Optically Shallow Waters from Multispectral Imagery without Ground Data. *Remote Sens.* **2021**, *13*, 1169. [CrossRef]
20. Liu, Y.; Zhao, J.; Deng, R.; Liang, Y.; Gao, Y.; Chen, Q.; Xiong, L.; Liu, Y.; Tang, Y.; Tang, D. A Downscaled Bathymetric Mapping Approach Combining Multitemporal Landsat-8 and High Spatial Resolution Imagery: Demonstrations from Clear to Turbid Waters. *ISPRS J. Photogramm. Remote Sens.* **2021**, *180*, 65–81. [CrossRef]
21. Giddens, J.; Kobayashi, D.R.; Mukai, G.N.M.; Asher, J.; Birkeland, C.; Fitchett, M.; Hixon, M.A.; Hutchinson, M.; Mundy, B.C.; O'Malley, J.M.; et al. Assessing the Vulnerability of Marine Life to Climate Change in the Pacific Islands Region. *PLoS ONE* **2022**, *17*, e0270930. [CrossRef]
22. Barnett, J.; Waters, E. Rethinking the Vulnerability of Small Island States: Climate Change and Development in the Pacific Islands. In *The Palgrave Handbook of International Development*; Springer: Berlin/Heidelberg, Germany, 2016.
23. Rapaport, M. *The Pacific Islands: Environment and Society, Revised Edition*; University of Hawaii Press: Honolulu, HI, USA, 2013; ISBN 978-0-8248-6584-9.
24. Xie, C.; Chen, P.; Pan, D.; Zhong, C.; Zhang, Z. Improved Filtering of ICESat-2 Lidar Data for Nearshore Bathymetry Estimation Using Sentinel-2 Imagery. *Remote Sens.* **2021**, *13*, 4303. [CrossRef]
25. Han, T.; Zhang, H.; Cao, W.; Le, C.; Wang, C.; Yang, X.; Ma, Y.; Li, D.; Wang, J.; Lou, X. Cost-Efficient Bathymetric Mapping Method Based on Massive Active–Passive Remote Sensing Data. *ISPRS J. Photogramm. Remote Sens.* **2023**, *203*, 285–300. [CrossRef]

26. Xie, C.; Chen, P.; Zhang, S.; Huang, H. Nearshore Bathymetry from ICESat-2 LiDAR and Sentinel-2 Imagery Datasets Using Physics-Informed CNN. *Remote Sens.* **2024**, *16*, 511. [CrossRef]
27. Xi, X.; Chen, M.; Wang, Y.; Yang, H. Band-Optimized Bidirectional LSTM Deep Learning Model for Bathymetry Inversion. *Remote Sens.* **2023**, *15*, 3472. [CrossRef]
28. Bernardis, M.; Nardini, R.; Apicella, L.; Demarte, M.; Guideri, M.; Federici, B.; Quarati, A.; De Martino, M. Use of ICEsat-2 and Sentinel-2 Open Data for the Derivation of Bathymetry in Shallow Waters: Case Studies in Sardinia and in the Venice Lagoon. *Remote Sens.* **2023**, *15*, 2944. [CrossRef]
29. Xie, J.; Zhong, J.; Mo, F.; Liu, R.; Li, X.; Yang, X.; Zeng, J. Denoising and Accuracy Evaluation of ICESat-2/ATLAS Photon Data for Nearshore Waters Based on Improved Local Distance Statistics. *Remote Sens.* **2023**, *15*, 2828. [CrossRef]
30. Ma, Y.; Xu, N.; Liu, Z.; Yang, B.; Yang, F.; Wang, X.H.; Li, S. Satellite-Derived Bathymetry Using the ICESat-2 Lidar and Sentinel-2 Imagery Datasets. *Remote Sens. Environ.* **2020**, *250*, 112047. [CrossRef]
31. Vermote, E.F.; Tanre, D.; Deuze, J.L.; Herman, M.; Morcette, J.-J. Second Simulation of the Satellite Signal in the Solar Spectrum, 6S: An Overview. *IEEE Trans. Geosci. Remote Sens.* **1997**, *35*, 675–686. [CrossRef]
32. Hedley, J.D.; Harborne, A.R.; Mumby, P.J. Technical Note: Simple and Robust Removal of Sun Glint for Mapping Shallow-water Benthos. *Int. J. Remote Sens.* **2005**, *26*, 2107–2112. [CrossRef]
33. Sun, W.; Chen, B.; Messinger, D.W. Nearest-Neighbor Diffusion-Based Pan-Sharpening Algorithm for Spectral Images. *Opt. Eng.* **2014**, *53*, 013107. [CrossRef]
34. Pasquarella, V.J.; Brown, C.F.; Czerwinski, W.; Rucklidge, W.J. Comprehensive Quality Assessment of Optical Satellite Imagery Using Weakly Supervised Video Learning. In Proceedings of the 2023 IEEE/CVF Conference on Computer Vision and Pattern Recognition Workshops (CVPRW), Vancouver, BC, Canada, 17–24 June 2023; pp. 2125–2135.
35. Wu, H.; Li, Z.-L. Scale Issues in Remote Sensing: A Review on Analysis, Processing and Modeling. *Sensors* **2009**, *9*, 1768–1793. [CrossRef] [PubMed]
36. Dong, P.; Gao, L.; Zhan, W.; Liu, Z.; Li, J.; Lai, J.; Li, H.; Huang, F.; Tamang, S.K.; Zhao, L. Global Comparison of Diverse Scaling Factors and Regression Models for Downscaling Landsat-8 Thermal Data. *ISPRS J. Photogramm. Remote Sens.* **2020**, *169*, 44–56. [CrossRef]
37. Kustas, W.P.; Norman, J.M.; Anderson, M.C.; French, A.N. Estimating Subpixel Surface Temperatures and Energy Fluxes from the Vegetation Index–Radiometric Temperature Relationship. *Remote Sens. Environ.* **2003**, *85*, 429–440. [CrossRef]
38. Martin, J.; Eugenio, F.; Marcello, J.; Medina, A. Automatic Sun Glint Removal of Multispectral High-Resolution Worldview-2 Imagery for Retrieving Coastal Shallow Water Parameters. *Remote Sens.* **2016**, *8*, 37. [CrossRef]
39. Xia, H.; Li, X.; Zhang, H.; Wang, J.; Lou, X.; Fan, K.; Shi, A.; Li, D. A Bathymetry Mapping Approach Combining Log-Ratio and Semianalytical Models Using Four-Band Multispectral Imagery Without Ground Data. *IEEE Trans. Geosci. Remote Sens.* **2020**, *58*, 2695–2709. [CrossRef]


**Disclaimer/Publisher's Note:** The statements, opinions and data contained in all publications are solely those of the individual author(s) and contributor(s) and not of MDPI and/or the editor(s). MDPI and/or the editor(s) disclaim responsibility for any injury to people or property resulting from any ideas, methods, instructions or products referred to in the content.